Experimental Thermal and Fluid Science 128 (2021) 110438

Contents lists available at ScienceDirect

Experimental Thermal and Fluid Science

journal homepage: www.elsevier.com/locate/etfs

Heat transfer characteristics of an impinging swirling inverse diffusion butane/air flame jet

L.L. Dong [a,b,*], C.S. Cheung [b], C.W. Leung [b]

[a] Department of Chemical Engineering, University of Birmingham, UK
[b] Department of Mechanical Engineering, The Hong Kong Polytechnic University, Hong Kong, China

ARTICLE INFO

Keywords:
Inverse diffusion flame
Heat transfer enhancement
Swirling flame jet

ABSTRACT

This paper presents an experimental study to explore the feasibility of utilizing a swirling inverse diffusion flame (IDF) jet for impingement heating. The investigation concentrates on the impinging flame structure and impingement heat transfer. The effects of air swirling, the air jet Reynolds number, Re_a, the global equivalence ratio, Φ, and the non-dimensional burner-to-plate distance, H/d_a, on the impinging flame shape and impingement heat transfer are investigated experimentally. The Experiments show that introduction of air swirling can either enhance or reduce the heat transfer rate depending on operating condition. Under-swirling produces no evident heat transfer enhancement due to insufficient air/fuel mixing, while over-swirling reduces heat transfer rate because of the dilution of the entrained cold ambient air. Heat transfer enhancement is achieved with the appropriate level of air swirling when the complete combustion occurs in the inner reaction zone around a stoichiometric condition. The investigation shows that the impinging inverse flame jet with an appropriate level of air swirling possesses the advantages of both premixed and diffusion flame jets with blue appearance, ultra-low NO_x emission, high flame temperature, good self-stabilization capability, and enhanced heat transfer rate. Therefore, it is a desirable option for impingement heating applications.

1. Introduction

Impinging flame has been widely used in domestic and industrial applications due to its enhanced convective heat transfer rate. Previous studies have focused on its heat transfer characteristics [1–3], pollutants emission characteristics [4–7], and flow and flame structure [8–10].

Premixed or partially premixed flame is often employed in impingement heating applications due to its high flame temperature and less or no soot emission [11–12]. However, several concerns are accompanied such as danger of flashback when flame speed is higher than the premixed fuel/air mixture velocity, and poor flame stability without external help. Normal diffusion flame is safe in essence, but it has low heat release rate and excess soot emission, which makes it a rare selection for impingement heating. In order to address these concerns, an inverse diffusion flame jet is resorted to. The present experimental study is aimed to explore the feasibility of swirling inverse flame jet for impingement heating, and thus to provide a desirable alternative to the conventional premixed flame jet.

Impinging swirling jet has been investigated for different purposes. Introduction of swirling to the isothermal impinging jet is used to obtain a more uniform heat transfer rate, and thus to reach a better cooling effect in electronic-cooling applications [13–15]. Introduction of swirling flow to free flame jet is aimed to either obtain a more stabilized flame or reduce NO_x emission [16–19,21]. Swirling flow is widely used to enhance the flame stability through the swirl-induced recirculation zone which carries the hot combusted gas downstream backwards to mix with the cold gas mixture. Feikema et al. [16] reported that introduction of swirling flow enhances the blow-out limits of the diffusion flame jet studied. Chan et al. [20] found that weak swirling flow is able to stabilize premixed flames. Huang et al. [22] have found that introduction of swirling can produce more uniform hat flux distribution along the impingement plate when studying a laminar premixed impinging flame jet. Recently, the heat transfer characteristics of a pair of premixed swirling flame jets have been investigated and reported [24–25]. Little work has been done to study the effect of swirling flow on the impinging IDF jet for rapid heating.

The previous studies by the authors have found that under certain operating conditions, introduction of swirling air flow can change the flame structure from a yellow diffusion flame to a blue premixed flame. In the meantime, swirling flame jet can achieve similar level of maximum flame temperature as that in the non-swirling flame jet, but

* Corresponding author at: Department of Chemical Engineering, University of Birmingham, UK.
E-mail address: l.dong@bham.ac.uk (L.L. Dong).

https://doi.org/10.1016/j.expthermflusci.2021.110438
Received 10 December 2020; Received in revised form 27 April 2021; Accepted 10 May 2021
Available online 23 May 2021

Nomenclature

d	air port diameter (m)
H	distance between the nozzle and the impingement plate (m)
P	static wall pressure (Pa)
$\dot{q}$	heat flux density(w/m^2)
r	radial distance from stagnation point (m)
Re	Reynolds number$(=u_a d_a/v_a)$
T	temperature (K)
u	Velocity(m/s)

Greek symbols

v	kinematic viscosity(m^2/s)
Φ	equivalence ratio (= (stoichiometric air/fuel volume ratio)/(actual air/fuel volume ratio))

Subscripts

a	air jet
at	atmospheric condition
w	impingement plate

emit much less NO_x due to the reduced flame length and residence time. It has been found that the blue swirling IDF jet is desirable for impingement heating. To understand more about the heat transfer characteristics of this blue swirling IDF, the current study focuses on the impinging flame structure and impingement heat transfer. Effects of air swirling, H/d_a, Re_a, and ϕ on the heat transfer rates are studied and discussed.

2. Experimental setup and uncertainty analysis

The experimental setup and the coordinate system are shown schematically in Fig. 1(a). The IDF is produced by a perforated brass burner with a 6 mm-diameter air port in the center surrounded by a row of 6 evenly distributed fuel ports of 3.4 mm in diameter. The center-to-center distance between the central air port and each fuel port is 8 mm. The burner head has a length of 35 mm and diameter of 40 mm. The swirling air flow is produced by a vane swirler with the swirl number of 0.43, which is of 6 mm in diameter and 12 mm in length. It is mounted flush inside the air port, with the vane angle of 45°. The schematic of the burner head with the air/fuel ports is shown in Fig. 1(b). Metered air was directly delivered to the IDF burner, while the metered butane gas was divided into two lines to enter the settling chamber in opposite directions. The distance between the inlets of the fuel gas is 40 mm. The opposite entry of the fuel gas is designed to obtain high level of turbulence before exiting. The augmented free stream turbulence will enhance the mixing of the fuel with the air after being issued. The IDF burner is fixed on a 3-dimensional positioner which could be moved freely. The IDF is enclosed with screen mesh to minimize the disturbance of the surrounding air flow. Gas samples within the flame are extracted by a quartz tube with an inner diameter of 1 mm and outer diameter of 2 mm, which is connected with a long flexible tube in the other end to cool the sampled gas flowing inside before entering into the gas analyzers.

The flame impingement surface is a rectangular copper plate of 200 mm long, 200 mm wide, and 8 mm thick. It is evenly cooled on the backside by a cooling water jacket. Copper is selected because of its excellent thermal conductivity. The top plate of the cooling water jacket is made of plexiglass to enable the water flow visible. After any change in the operating condition, measurements are only made after the steady-state condition has been established again and the exit temperature of the cooling water has been stabilized. The local heat flux from the flame to the plate is measured with a coated Vatell HFM-6

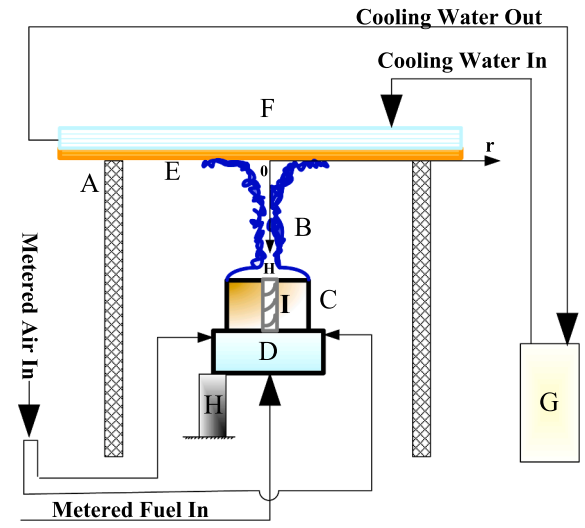

A: Screen Mesh **B: Inverse Diffusion Flame**

C: Burner Head **D: Settling Chamber**

E: Brass Impingement Plate **F: Cooling Water Jacket**

G: Thermalstat **H: 3-D Positioner**

I: Swirler

Fig. 1a. Schematic of the Test Rig and the Coordinate System.

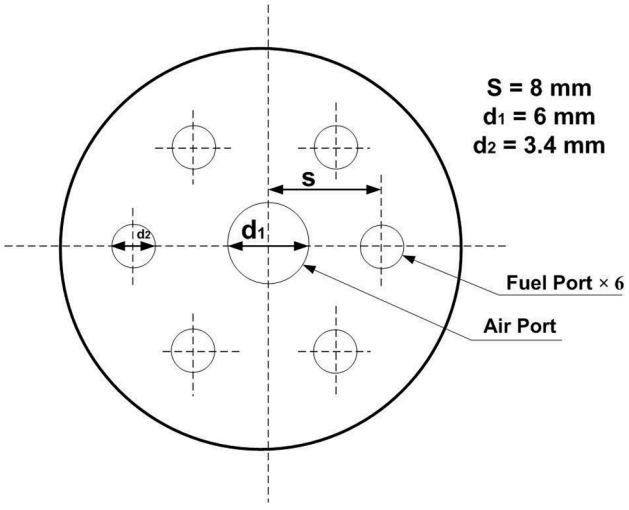

Fig. 1b. Schematic of the IDF Burner Head.

microsensor installed inside the impingement plate. The sensor surface is flush with the front side of the plate facing the flame. The output voltage signal is recorded by a stand-alone IOtech data acquisitor after being amplified by an AMP-6 amplifier. The radial heat flux distribution is obtained with 1 mm apart by moving the burner positioner horizontally. A single pressure tap of 1 mm diameter is drilled through the copper plate at its center. The radial pressure distributions along the plate are obtained by moving the three-dimensional burner positioner in the x-, y- and z-directions, while the plate remained stationary. The pressure tap is connected via a flexible tube to an inclined differential manometer with an accuracy of 2% of the full scale. Direct images of the flames are obtained with a digital camera. The flame temperature is

measured by a B-type uncoated bare wire thermocouple with the bead diameter of 0.5 mm. The thermocouple is fixed on a still holder. By moving the burner, the radial and axial flame temperature distributions are measured. The same IOtech data acquisitor is used to record the flame temperature along with heat flux. Corrections for temperatures over 300 °C are made to compensate for the radiative and convective heat exchanges from the thermocouple bead with the method suggested by Bradley and Matthews [33]. The emissivity of the thermocouple bead is assumed to be a constant as no soot accumulation is found in the present study. An emissivity of 0.14 is selected as recommended for uncoated Type B thermocouple by Sparrow and Cess [34]. The maximum temperature corrected is 132 °C.

To ensure the repeatability, each set of experiments was conducted two times and the averaged values are reported and employed to perform the uncertainty analysis. The uncertainty analysis is performed with the method of Kline and McClintock [23]. With a 95% confidence level, the uncertainty of the heat flux measurement ranges between 1.2% and 8.5%, respectively.

3. Flame and thermal structures of free swirling IDF jet

The direct photos of the swirling IDF jets and non-swirling IDF jets under different Φ are shown in Figs. 2(a) and 2(b), respectively. It can be seen from Figs. 2(a) and 2(b) that the flames have unique appearances. Irrespective of the Φ, all the flames can be divided into three parts, i.e., base flame, flame neck and flame torch. The base flame is a diffusion flame formed by the combustion of the six fuel jets before they reach the flame neck where meeting with the central air jet. The fuel jets are sucked by the central high speed air jet and flow inwards after discharging and finally impinge on the central air jet, where a contracted flame neck is formed. Due to the direct impingement of the fuel jets, air/fuel mixing occurs in the flame neck. Beyond that, the gas mixture marches further downwards forming a flame torch. It can also be observed from Fig. 2(a) that in the range of $\Phi = 0.6$ to $\Phi = 2.17$, the flame torch can be classified into two types. The first type is a blue premixed flame when $\Phi \leqslant 1.2$. This premixed flame is formed due to the occurrence of complete mixing. Like Bunsen premixed flames, the premixed flame torch also has double layers, with an inner reaction zone and an outer diffusion layer. When Φ is increased to 1.6, yellow soot is observed on the top of the reaction zone, indicating a fuel-rich combustion. When Φ is further increased to 2.17, the second type of flame torch, i.e., a yellow plume flame, is formed on the top due to excessive fuel-rich condition.

To help further understand the effect of the air swirling on the flame shape, the non-swirling flames are shown in Fig. 2(b). The differences can be clearly observed in terms of flame appearance and flame length. Comparing to the swirling flame jet, the non-swirling flame jet is longer and thinner. On the whole, they are yellow in appearance except blue tips under the fuel-lean conditions due to the excess soot emission associated with incomplete fuel/air mixing in the flame neck when there is no air swirling to further enhance fuel/air mixing.

Therefore, air swirling can enhance the air/fuel mixing in the flame neck, and produce a premixed blue flame downwards, which is desirable for impingement heating. In the meantime, this IDF is still a diffusion flame in essence, which has no danger of flashback and has a better flame stability. The lean blow-off limit is as low as $\Phi = 0.01$ for both swirling and non-swirling IDFs over a wide range of Re_a from 500 to 10000, where only base flame exists with no flame neck due to extreme fuel-lean condition and all the fuel already consumed before impinging on the central air jet. Therefore, the current investigation is focused on blue swirling IDF for impingement heating purpose.

The temperature contours of the swirling and the non-swirling flame jets are shown in Figs. 3(a) and 3(b), to demonstrate their different thermal structures.

It can be seen from Fig. 3(a) that the temperatures in the base flame zone, which is below the flame neck, are generally low, with the coldest occurring in the flame center. This is attributed to the cold air jet which is not yet disturbed by the surrounding fuel jets. As a result, no combustion occurs in this region. Beyond the flame neck, this adverse radial temperature gradient disappears quickly and the flame temperature increases sharply and then reaches the highest value rapidly. This is the area between $y = 15\ mm$ and $y = 40\ mm$, where the primary chemical reaction occurs. This is also the region where the swirling-induced recirculating flow occurs. It has been found that swirling flame is characterized by the occurrence of a swirl-induced recirculating flow in the flame reaction zone, which carries the hot combusted gases backwards to mix with the cold unreacted gases [18,29,30]. As the result, a strong fuel/air mixing occurs in this region and the combustion is carried out in a premixed way, producing intense heat release rate and giving rise to high flame temperature.

As a comparison, the temperature contour of a non-swirling flame jet is shown in Fig. 3(b) under the same condition. It is observed that in general, the flame is thinner and the longer. Without air swirling, the influence of the cold central air jet on the flame thermal structure is more prominent than that with air swirling. The adverse radial temperature gradient persists until approximately $y = 80\ mm$, where the maximum flame temperature reaches. This is the result of the incomplete mixing of the air with the surrounding fuel jets due to the insufficient air suction and lack in swirling.

4. Nox emissions from the swirling IDF jet

The values of NOx emission index, $EINO_x$, and the comparison with those reported in literature, are shown in Fig. 4.

It is observed from Fig. 4 that the $EINO_x$ is higher from non-swirling jet than that from the swirling jet. This difference is slight when $\phi = 0.6$ due to the low level of flame temperature. As increasing Φ, the difference in $EINO_x$ becomes larger. As shown previously in Fig. 3(a) and Fig. 3(b), the flame length of the swirling flame jet is much shorter than that of the non-swirling flame jet. Thus, the swirling flame jet has a much less residence time, which reduces the formation and eventual emission of NO_x. This effect has also been observed and reported in [16]

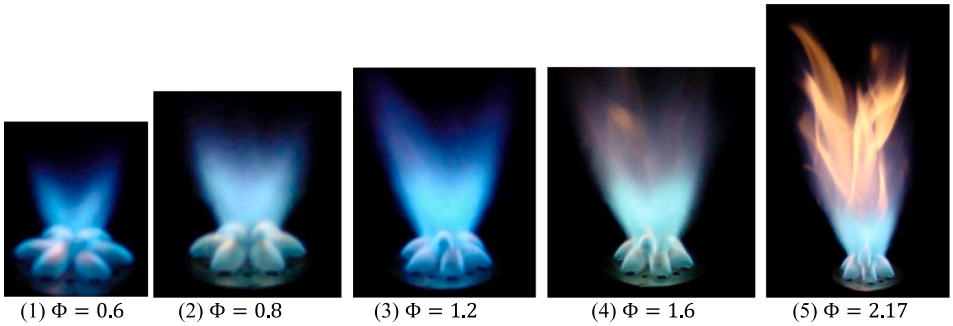

(1) Φ = 0.6 (2) Φ = 0.8 (3) Φ = 1.2 (4) Φ = 1.6 (5) Φ = 2.17

Fig. 2a. Flame Photograph at $Re_a =$ 6500 with Air Swirling.

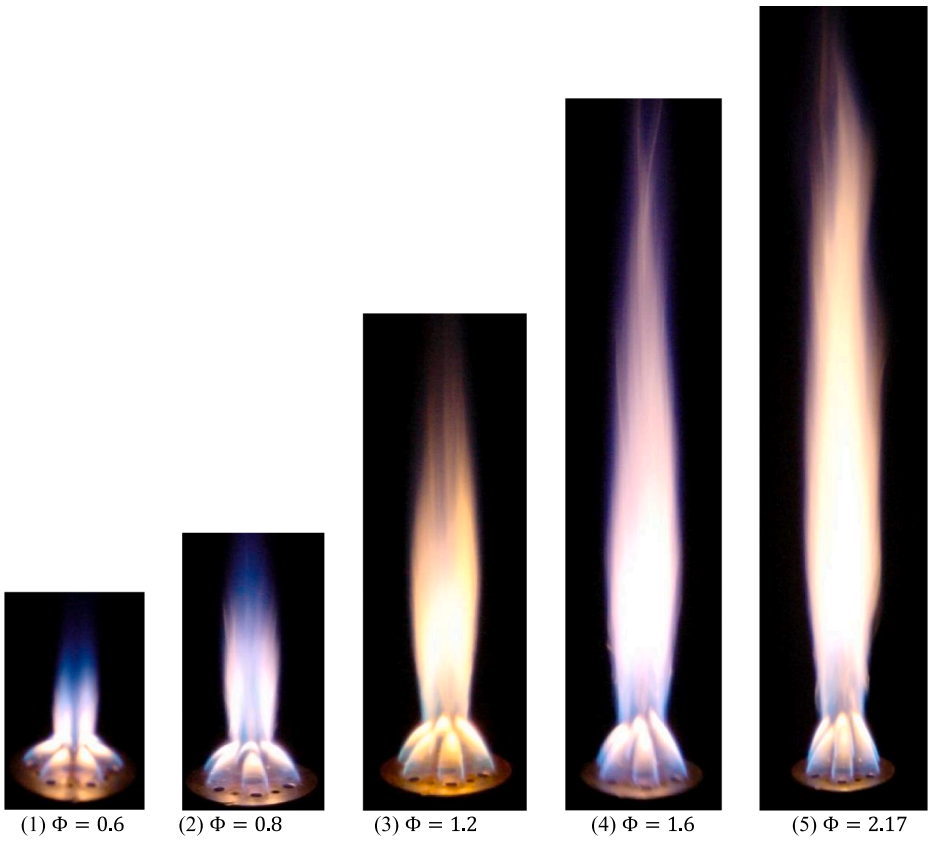

Fig. 2b. Flame Photograph at $Re_a =$ 6500 without Air Swirling.

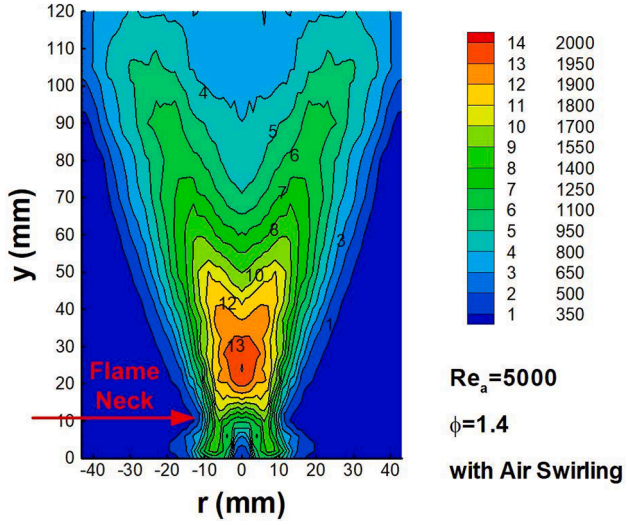

Fig. 3a. Temperature Contour of Swirling Flame.

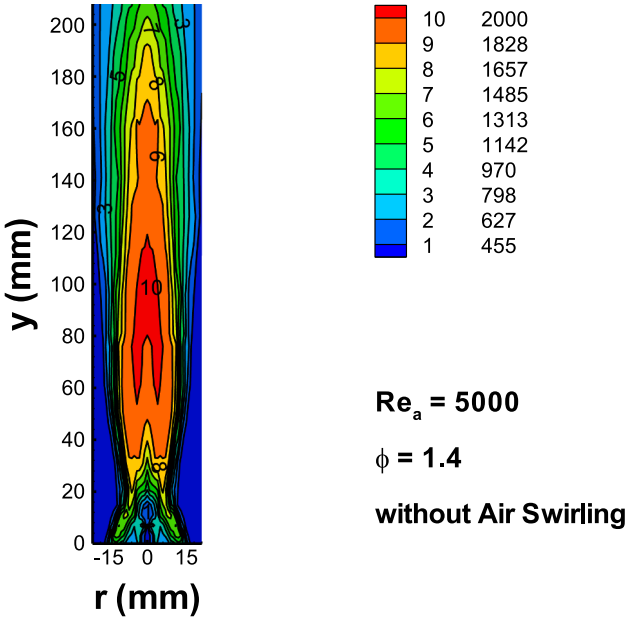

Fig. 3b. Temperature Contour of Non-Swirling Flame.

and [29].

It can also be seen from Fig. 4 that $EINO_x$ increases with the increase in Φ. This is due to the increased flame length, and thus the prolonged residence time. The maximum $EINO_x$ from the current swirling IDF is 1.6, which is lower than 2.5 from a partially premixed flame when $\phi = 1.0$, as reported by Lyle et al. [28]. Mahesh et al. [27] reported a maximum $EINO_x$ of 4.0 for their co-flowing IDF. Laurendeau [31] reported a maximum $EINO_x$ of around 2.5 for their IDF in air-staged burner, and Stansel et al. [32] reported a maximum $EINO_x$ of 2.8 from an air-staged diffusion flame. Therefore, it can be seen that the current swirling IDF can produces very low level of NO_x emission, which makes it a desirable choice for impingement heating.

5. Flame structures of the impinging swirling IDF jet

The direct photos of the impinging swirling IDF jet are shown from Figs. 5–7. As a comparison, the photos of the non-swirling impinging jets are shown as well.

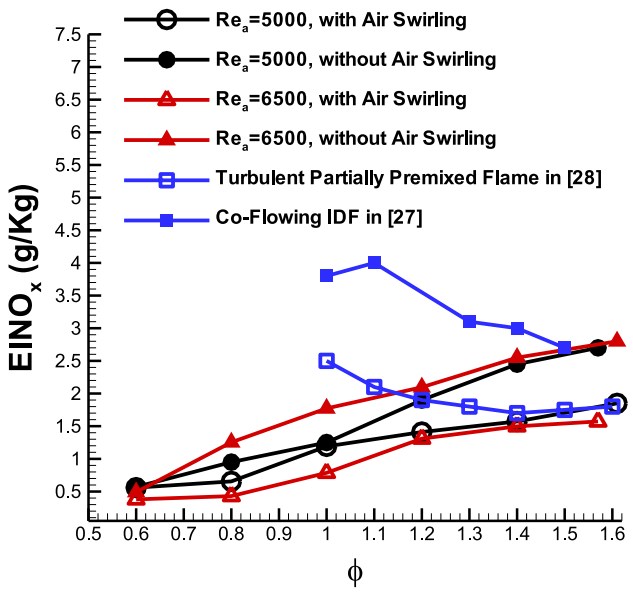

Fig. 4. Comparison of EINO$_x$ with and without Air Swirling.

The flame shapes under different ϕ with and without air swirling are shown from Fig. 5(a)–(h). The ϕ varies from 0.8 to 1.6, where generally blue flame is produced for swirling IDF jet. The appearances of the flames without air swirling are shown from Fig. 5(a)–(d), respectively. It is observed that all the four flames are very luminous with yellow colour, especially along the trajectories of each fuel jet. The less strong suction produced by the central air jet results in an insufficient mixing of fuel and air in the flame neck, leaving unmixed fuel to continue marching downstream in a diffusion combustion mode, thus emitting more soot than the regions between them. As increasing ϕ, the flame becomes longer, resulting in a direct impingement of the central cold air/fuel mixture on the plate, which is dark due to the lack in chemical reaction, as observed clearly in Fig. 5(c) and Fig. 5(d). As a comparison, the flame appearances of the swirling IDF jet under the same operating conditions are shown from Fig. 5(e)–(h), respectively. It is observed that the flames are all blue under $\phi = 0.8$ and $\phi = 1.2$. When ϕ is increased to 1.4, a slight and intermittent yellow soot emission is observed visually. When ϕ is further increased to 1.6, more soot is emitted on the top of the flame, but the flame on the whole remains blue. Through the range of ϕ, the base flame, flame neck and the bottom part of the flame torch (the recirculation zone) remains blue.

The flame appearances under different H/d_a are shown From Fig. 6 (a)–(h), respectively. For the impinging swirling jet, H/d_a is varied from 3, where the inner recirculating reaction zone impinges on the plate, to 9, where the outer flame (or the flame wings) impinges on the plate. As a comparison, two photos of the flames without air swirling are shown in Fig. 6(g) and (h). It is found from Fig. 3(a) that under small H/d_a of 3, the inner reaction zone directly contacts the impingement plate. When gradually increasing H/d_a to 5, it is observed from Fig. 6(c) that the tip of the inner reaction zone is very close to the impingement plate. Further increase in H/d_a leads to a direct impingement of the outer flame on the plate, as shown from Fig. 6(d)–(f). In contrast, the impinging non-swirling flame jets are typical diffusion flames with bright yellow colour except at the base of the flame close to the burner exit, as shown in Fig. 6(g) and (h).

The effects of the Re$_a$ on the impinging flame appearances are shown in Fig. 7. It is observed that the impinging flame jet is generally yellow when $Re_a = 3000$. The flame turns blue when increasing Re$_a$ to 5000 and further to 6500 due to the stronger suction of the air jet and the enhanced fuel/air mixing.

6. Local heat transfer characteristics

The radial distributions of the static wall pressure and the heat transfer rate with the variations of Φ, Re$_a$ and H/d_a are shown from Figs. 8–10. To facilitate the comparison with the static wall pressures reported from literature, the static wall pressure, P_w, is normalized by the atmospheric pressure, P_{at}, as shown in the following diagrams.

6.1. Effects of Φ on P_w and $\dot{q}$

The variations of the wall pressure with the Φ are shown in Fig. 8(a), where Φ is ranged from 0.8 to 1.82. It is observed from Fig. 8(a) that in all the three conditions, the distribution lines are all characterized with a low P_w at the stagnation point, two symmetrical maximum P_w some distance away from the stagnation point. This saddle-shaped trend line corresponds to the recirculating flow zone. Visualization of the impinging swirling isothermal jet by Huang et al. [13] showed that the exiting spiral flow formed a continuous flow cone after discharged. They also found that the location where the highest heat transfer rate occurs is also the position which the jet flow cone impinges on. Outside and inside the flow cone, flow mixing is reduced, leading to a decreased heat transfer rate. In the present swirling flame jet, the flow cone corresponds to the recirculating inner reaction zone. The maximum P_w occurs when the flow cone, i.e., the boundary of the inner reaction zone, impinges on the plate. The location of the peak P_w is also the point where the maximum axial velocity occurs in the jet when impinging on the plate. The region inside the inner reaction zone is characterized by recirculating flow. Therefore, the flow in the jet centre encounters the backward flow when marching downstream, which thus reduces the axial jet velocity before impinging on the plate. As a result, a minimum P_w is obtained at the stagnation point. It is also observed from Fig. 8(a) that as increasing Φ, the location where the maximum P_w occurs moves a little inwards from $r/d_a = 2.3$ under $\phi = 0.8$ to $r/d_a = 1.3$ under $\phi = 1.82$. This indicates a decrease in the cross-sectional area of the recirculating zone. This is because the radial velocity of the air jet is decreasing faster as a result of intensified mixing with more surrounding fuel under larger Φ. Further increase in the radial distance results in a rapid decrease in P_w beyond the peak value.

The radial distributions of $\dot{q}$ under different Φ are shown in Fig. 8(b). It is found that like the distribution trend of P_w, $\dot{q}$ also varies following saddle-shaped trend line when Φ is increased from 0.8 to 1.82. This distribution trend is also found in the previous studies on swirling isothermal jet [1,13]. $\dot{q}$ reaches a minimum value at the stagnation point. Then it increases gradually to a peak value some distance away. After that, $\dot{q}$ decreases monotonically with further increase in r/d_a. Further observation in Fig. 5(b) shows that the locations where the maximum $\dot{q}$ occur under $\phi = 0.8$, $\phi = 1.4$, and $\phi = 1.82$ are r/d$_a$ = 2.3, r/d$_a$ = 2, and r/d$_a$ = 1.3, respectively. These locations coincide with those where the peak P_w occur, as shown in Fig. 8(a). In the inner reaction zone, the flame temperature distribution line has a bell-shape, with the maximum in the flame centre. Considering these two factors, it is clear that the maximum $\dot{q}$ occurs where the maximum P_w occurs, i.e., the location where the maximum axial velocity is achieved in the impinging flame jet, rather than the stagnation point where the maximum flame temperature is reached. This indicates that the high turbulence level in the region around the peak P_w due to large impinging velocity dominates the convective heat transfer rate. It is also observed from Fig. 8(b) that $\dot{q}$ increases steadily as increasing Φ from 0.8 to 1.4. This is mainly due to the steady increase in flame temperature with increasing Φ. On the other hand, the value of P_w, i.e., the level of the turbulence, is also increased from $\phi = 0.8$ to $\phi = 1.4$, as shown in Fig. 8(a). The maximum $\dot{q}$ is achieved under $\phi = 1.4$. This is the condition where the flame inner reaction zone is just reaching the impingement plate, as shown in Fig. 6 (c), which is featured with high flame temperature and high jet impingement velocity. It is also found from Fig. 8(b) that as further increasing Φ to 1.82, there is a little decrease in peak $\dot{q}$ due to the

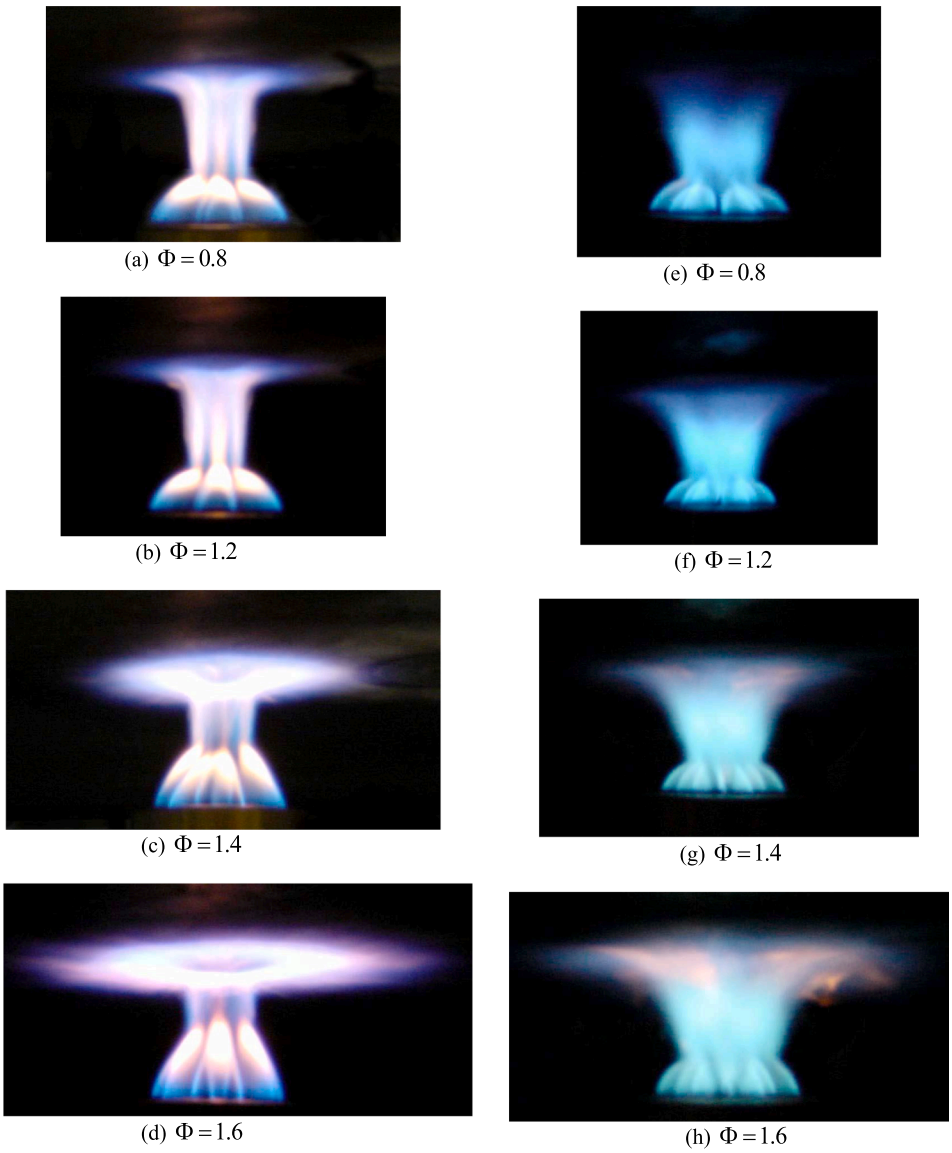

Fig. 5. Photos of the Impinging IDFs with and without Air Swirling under $Re_a =$ 6500 and $H/d_a = 5$. – (d): without Air Swirling. (e) – (h): with Air Swirling.

decrease in flame temperature associated with excess fuel supply and incomplete combustion.

6.2. *Effects of Re_a on p_w and $\dot{q}$*

The variation of P_w with Re_a is shown in Fig. 9(a). It is again observed that the swirling air flow results in a minimum P_w in the stagnation point and two peak values some distance away under all Re_a from 3000 to 6500. It is also observed that P_w is increased gradually with the increase in Re_a, which is more evident in the region of $-2 < r/d_a < 2$. This is the result of the increased air jet velocity. When Re_a is increased from 3000 to5000, P_w is generally increased all the way with the increase in Re_aexcept under $Re_a = 6500$, where P_w drops sharply from the peak value and reaches zero at around $r/d_a = \pm 5$, indicating an early occurrence of the wall jet flow.

The radial distributions of $\dot{q}$ when Re_a is increased from 3000 to 6500 are shown in Fig. 9(b). It is observed that $\dot{q}$ increases monotonically with increasingRe_a from 3000 to 5000 due to the increased air jet velocity and turbulence level. Then $\dot{q}$ starts to decrease when Re_a is further increased to 6500. This is resulted from the decreased flame temperature because of the dilution of the excess cold entrained air. Therefore, we can conclude that the enhanced heat transfer occurs when the jet velocity or the turbulence level is high, or a nearly stoichiometric combustion is reached before impingement. In comparison, unlike the impinging flame jet, a monotonic increase in local Nusselt number with increase in Re in the impinging swirling isothermal air jet has been found [1], where the turbulence effect is dominant due to the absence of chemical reaction.

The variation of the radial $\dot{q}$ with Re_a for non-swirling flame jet is shown in Fig. 9(c). It is observed that under all the four conditions, the distribution lines are also saddle-shaped, similar to those with swirling flame jets. However, this is due to different reason. The lower level of $\dot{q}$ around the stagnation point is due to the presence of the cold central air. Thanks to the much weakened mixing of air and surrounding fuel jets with the absence of the swirling flow, the flame temperature in the centre is lower than the peak value some distance away. As a result, the heat flux at the stagnation point comes as a minimum despite the high impinging velocity and turbulence level in the stagnation region. It is also observed from Fig. 9(c) that in the region between the two peak $\dot{q}$, $\dot{q}$ is generally increased with the decrease in Re_a. This is the result of the stronger influence of the cold central air jet under higher Re_a. The peak $\dot{q}$ occurs where combustion takes place, which leads to increased flame temperature and enhanced heat flux. Beyond that, the heat flux starts to decrease as the deflected flame jet spreads further outwards along the plate. In the meantime, it is also observed that $\dot{q}$ is increased with

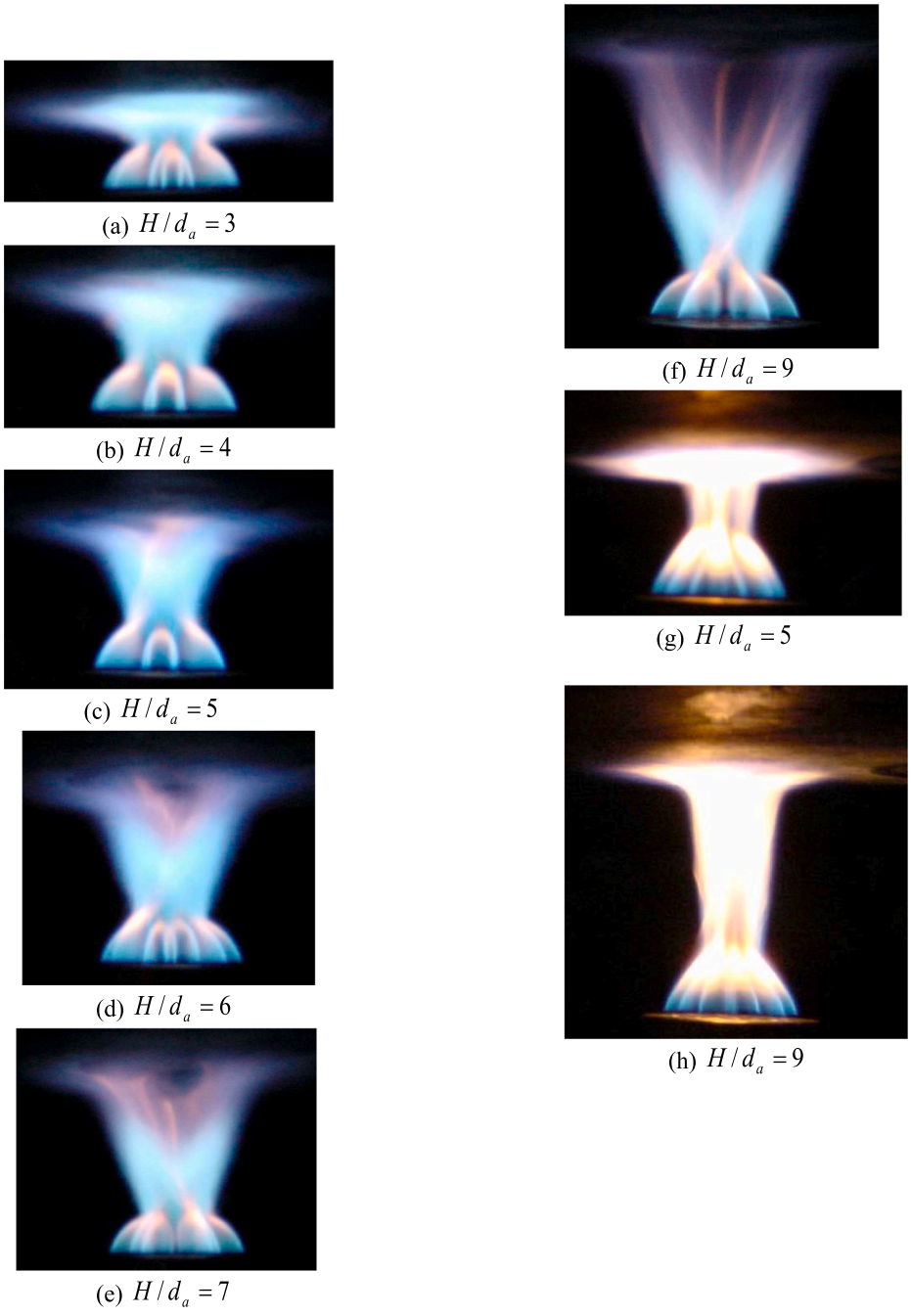

Fig. 6. Photos of the Impinging IDFs under $Re_a =$ 5000 and $\Phi = 1.4$. – (f): with Air Swirling. (g) – (h): without Air Swirling.

increasing Re_a. This is due to the increased flame temperature and turbulence level.

6.3. Effects of H/d_a on P_w and $\dot{q}$

The variations of P_w and $\dot{q}$ with H/d_a under $Re_a = 5000$ are shown from Fig. 10(a)–(c), respectively, while Fig. 10(d) and (e) present the distributions of P_w and $\dot{q}$ when H/d_a is increased from 3 to 9 under $Re_a =$ 6500.

The radial distributions of P_w under different H/d_a in the swirling flame jet are shown in Fig. 10(a). The selected H/d_a are 3, 5, and 9, representing small, moderate and large distances. For comparison, the radial distributions of P_w when there is no air swirling are shown in Fig. 10(b). It is observed from Fig. 10(a) that P_w decreases steadily with the increase in H/d_a. This is because the impinging flame jet entrains the surrounding air all the way before it reaches the plate, which reduces the jet momentum and jet velocity. On the other hand, the locations where the peak P_w occur moves outwards as increasing H/d_a from around $r/d_a = \pm 1.0$ under $H/d_a = 3$ to around $r/d_a = \pm 2.3$ under $H/d_a = 9$. This is because that the longer travelling distance of the jet before impingement allows the recirculation flow cone to expand radially along the way, resulting in the outward displacement of the peak P_w, which is coincident with the location where the recirculating flow cone impinges on the plate.

For the non-swirling impinging flame jet, the distribution trend line of P_w is bell-shaped, as shown in Fig. 10(b). P_w increases monotonically with the increase in H/d_a in the stagnation region. Then it decreases rapidly to nearly zero some distance away from the stagnation point in the region of $-2 < r/d_a < -1$ and $1 < r/d_a < 2$. It is also observed that P_w decreases faster under higher H/d_a. P_w reaches almost zero at around r/

(a) $Re_a = 3000$

(b) $Re_a = 5000$

(c) $Re_a = 6500$

Fig. 7. Photos of the Impinging IDFs under $\varphi = 1.4$, $H/d_a = 5$

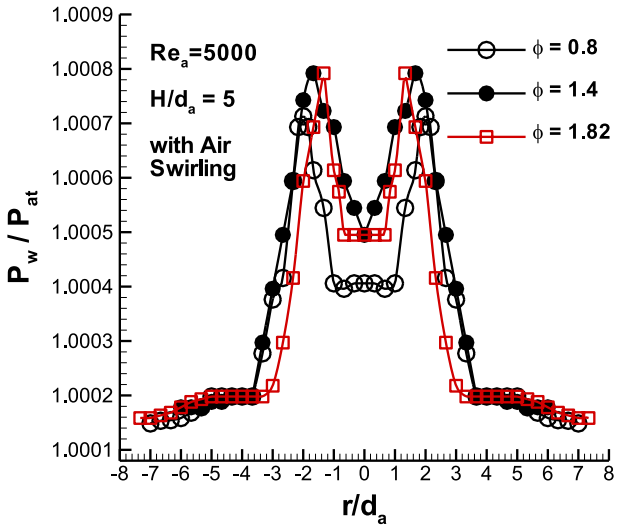

(a) Variations of the Wall Pressure Distributions with Φ

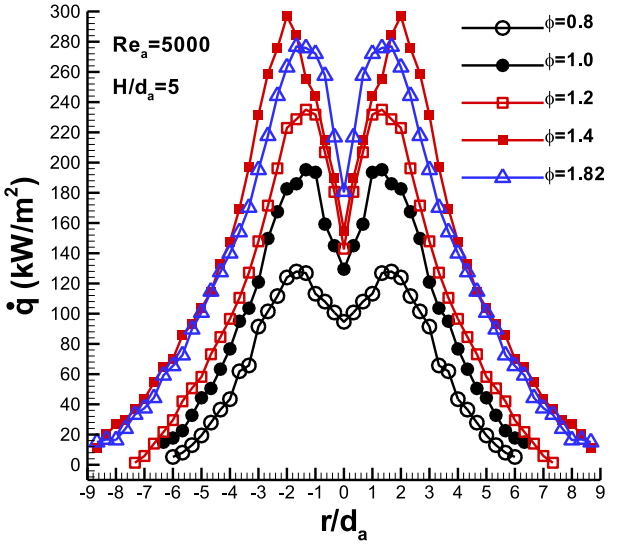

(b) Variations of the Radial Heat Flux Distribution with Φ

Fig. 8. Effects of the Φ on $\dot{q}$ and P_w

d_a=±1.2 under $H/d_a = 3$, while this occurs at around r/d_a=±1.4 under $H/d_a = 5$, and r/d_a=±1.8 under $H/d_a = 9$. This indicates a delayed occurrence of the wall jet region and accordingly a larger impingement region under higher H/d_a, which can exert influence on the heat transfer rate.

It can be seen from Fig. 10(b) that the maximum P_w/P_{at} for non-swirling flame jet decreases from 1.038 under $H/d_a = 3$ to 1.006 when $H/d_a = 9$. As a comparison, Markal [26] reported that the maximum P_w/P_{at} decreases from 1.012 under $H/d_a = 0.5$ to 1.006 under $H/d_a = 2.5$ for impinging air jet. The difference could be due to different air flow rate and burner type.

The variation of the radial distribution of $\dot{q}$ when H/d_a is increased from 3 to 9 is shown in Fig. 10(c). It is observed that under small H/d_a of 3, $\dot{q}$ is generally low due to the direct impingement of the inner reaction zone, as shown in Fig. 6(a). The cold impingement plate quenches the flame, resulting in an incomplete combustion close to the plate and the reduced flame temperature. Therefore, although the impinging jet velocity and the turbulence level is high in this case, the heat transfer rate still comes with a low level due to the reduced flame temperature associated with the incomplete combustion. As H/d_a is increased to 5, it is the high-temperature, freshly combusted gas that directly impinges on the plate. As a result, the enhanced flame temperature increases the heat transfer rate. As further increasing H/d_a, the flame temperature decreases gradually due to the entrainment of the cold ambient air, giving rise to decrease in $\dot{q}$.

The variations of the radial P_w and $\dot{q}$ with H/d_a under $Re_a = 6500$ are shown in Fig. 10(d) and (e), respectively. In general, a similar distribution trend is found as that under $Re_a = 5000$. It is observed from Fig. 10(d) that the peak P_w is higher than that under $Re_a = 5000$ given the same H/d_a, as shown in Fig. 10(a), indicating an increased impinging velocity and turbulence level. In the meantime, it is observed from Fig. 10(d) that the peak $\dot{q}$ comes lower than that under $Re_a = 5000$. This is due to the decreased flame temperature despite the enhanced turbulence level, as discussed before.

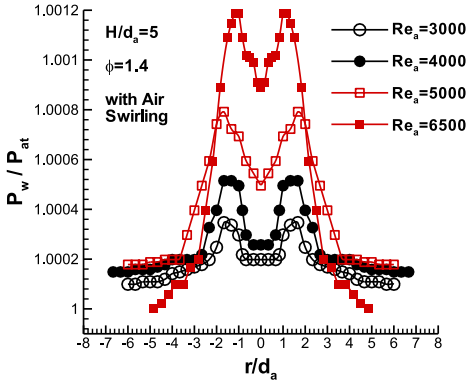

(a) Variations of the Wall Pressure Distribution with Re_a

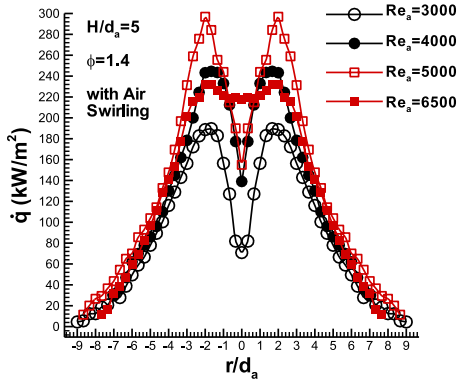

(b) Variations of the Radial Heat Flux Distribution with Re_a in the Swirling Flame Jet under $H/d_a = 5$

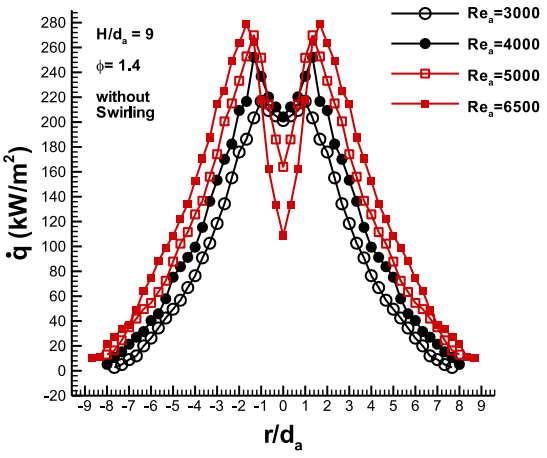

(c) Variations of the Radial Heat Flux Distribution with Re_a in the Non-Swirling Flame Jet under $H/d_a = 9$

Fig. 9. Effects of Re_a on $\dot{q}$ and P_w

6.4. Effects of air swirling on $\dot{q}$

To understand well the effects of air swirling on the heat transfer performance, the comparisons of the radial distributions of $\dot{q}$ from the impinging flame jets in the cases with and without air swirling are shown in Fig. 11. The comparisons are made under four Re_a ranging from 3000 to 6500. Due to the different flame structures and lengths of the impinging jets with and without air swirling, it is of less point to make a comparison under the same H/d_a. Therefore, the comparison of the local heat transfer distribution is made under the H/d_a where each maximized $\dot{q}$ is achieved in the two cases. The experiments show that these two $\mathrm{H/d_a}$ are 5 and 9 for the impinging jets with and without air swirling under $\mathrm{Re_a} = 5000$ and $\phi = 1.4$, respectively. For convenience, the $\dot{q}$ under the other three $\mathrm{Re_a}$ are also compared under these two H/d_a.

It is observed from Fig. 11(a) that under $\mathrm{Re_a} = 3000$, the highest $\dot{q}$ is occurred in the non-swirling flame jet when $H/d_a = 9$, while the lowest $\dot{q}$ is from the swirling flame jet under the same H/d_a. The introduction of the air swirling shows no heat transfer enhancement under this $\mathrm{Re_a}$. This is attributed to insufficient swirling intensity associated with low $\mathrm{Re_a}$. This under-swirling condition, i.e., when the swirling level is not high enough to give rise to stronger and thorough fuel/air mixing, leaves the flame to continue to be yellow to a large extent, as previously shown in Fig. 7(a). The incomplete combustion results in reduced flame temperature and thus the low level of $\dot{q}$. The flame length of the swirling jet is much shorter than that of the non-swirling jet. Therefore, the $\dot{q}$ from the swirling jet decreases significantly under larger H/d_a of 9 due to the reduced flame temperature. In the meantime, unlike the other cases, the $\dot{q}$ varies following a bell-shaped line for the swirling jet under $H/d_a = 9$. This indicates that the influence of the swirling flow has died out in this location.

When $\mathrm{Re_a}$ is increased to 4000, the similar comparisons are made, as shown in Fig. 11(b). It is observed that the highest $\dot{q}$ comes from both the swirling jet under $H/d_a = 5$ and the non-swirling jet under $H/d_a = 9$. The increased jet exiting velocity enhances the influence of the swirling flow and thus promotes the fuel/air mixing, giving rise to a more complete combustion than that under lower H/d_a. It is also observed that like the other three cases, the $\dot{q}$ from the swirling jet under $H/d_a = 9$ varies following a saddle-shaped trend line. This indicates the increased influence of the swirling flow cone. When $\mathrm{Re_a}$ is further increased to 5000, it is observed from Fig. 11(c) that the highest $\dot{q}$ occurs in the swirling jet under $H/d_a = 5$. Moreover, the local heat transfer rate under this condition comes higher all along the radial distance than that from the non-swirling jet under $H/d_a = 9$, where the maximized heat transfer rate occurs for non-swirling jet. This heat transfer enhancement in the swirling jet is due to the augmented flame temperature associated with nearly stoichiometric combustion in the reaction zone, as discussed before. When $\mathrm{Re_a}$ is further increased to 6500, it is observed that the swirling flame jet produces lower heat transfer rate than non-swirling flame jet. This is due to the reduced flame temperature caused by dilution of the cold entrained ambient air, as the result of over-swirling with too high swirling level. Therefore, so far it is clear that the effect of air swirling on the heat transfer performance of the impinging IDF jet is depending on $\mathrm{Re_a}$. Under low $\mathrm{Re_a}$ such as 3000, poor fuel/air mixing in the IDF jet requires higher level of swirling flow to enhance the mixing

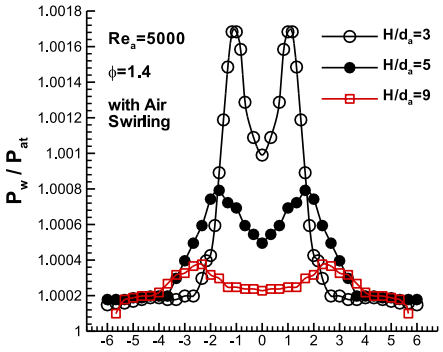

(a) Variations of the P_w with H/d_a under $Re_a = 5000$

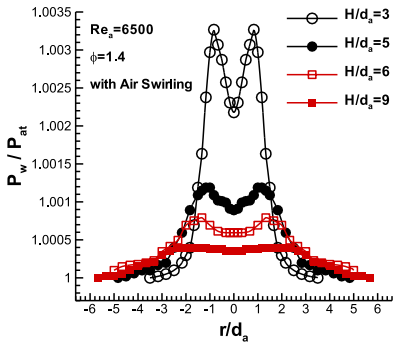

(d) Variations of the P_w with H/d_a under $Re_a = 6500$

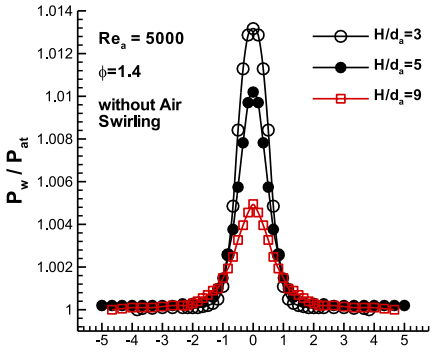

(b) Variations of the P_w with H/d_a without Air Swirling

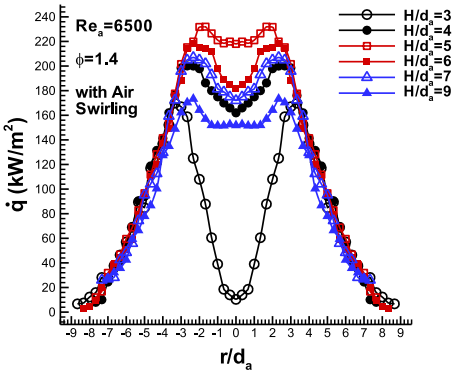

(e) Variations of the Radial Heat Flux Distribution with H/d_a in the swirling Flame Jet under $Re_a = 6500$

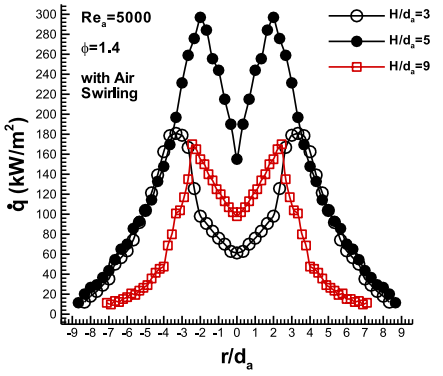

(c) Variations of the Radial Heat Flux Distribution with H/d_a in the Swirling Flame Jet under $Re_a = 5000$

Fig. 10. Effects of H/d_a on $\dot{q}$ andP_w

to achieve blue appearance and complete combustion. Insufficient swirling intensity is not able to change flame structure from a yellow diffusion flame to a blue premixed one due to insufficient fuel/air mixing. Relatively lower level of swirling flow is required when Re_a reaches as high as 6500. This is because fuel/air mixing is self-enhanced by the high air jet velocity. As a result, less higher swirling level is required to achieve a complete combustion around the stoichiometric condition. In short, by appropriately adjusting the value of the swirl intensity in response to different Re_a, heat transfer enhancement by introduction of air swirling can be achieved.

7. Conclusions

(1) Introduction of Air Swirling enhances fuel/air mixing in the IDF jet via the formation of recirculation zone close to the flame base. Appropriate level of swirling intensity can change the structure of the IDF from a yellow diffusion flame to a blue premixed one.

(2) The distribution of P_w follows a saddle-shaped trend line due to the presence of the recirculation zone inside the flow cone. This flow characteristics results in a similar saddle-shaped trend line for the radial distribution of $\dot{q}$ despite the bell-shaped variation of the flame temperature in the centre of the inner reaction zone.

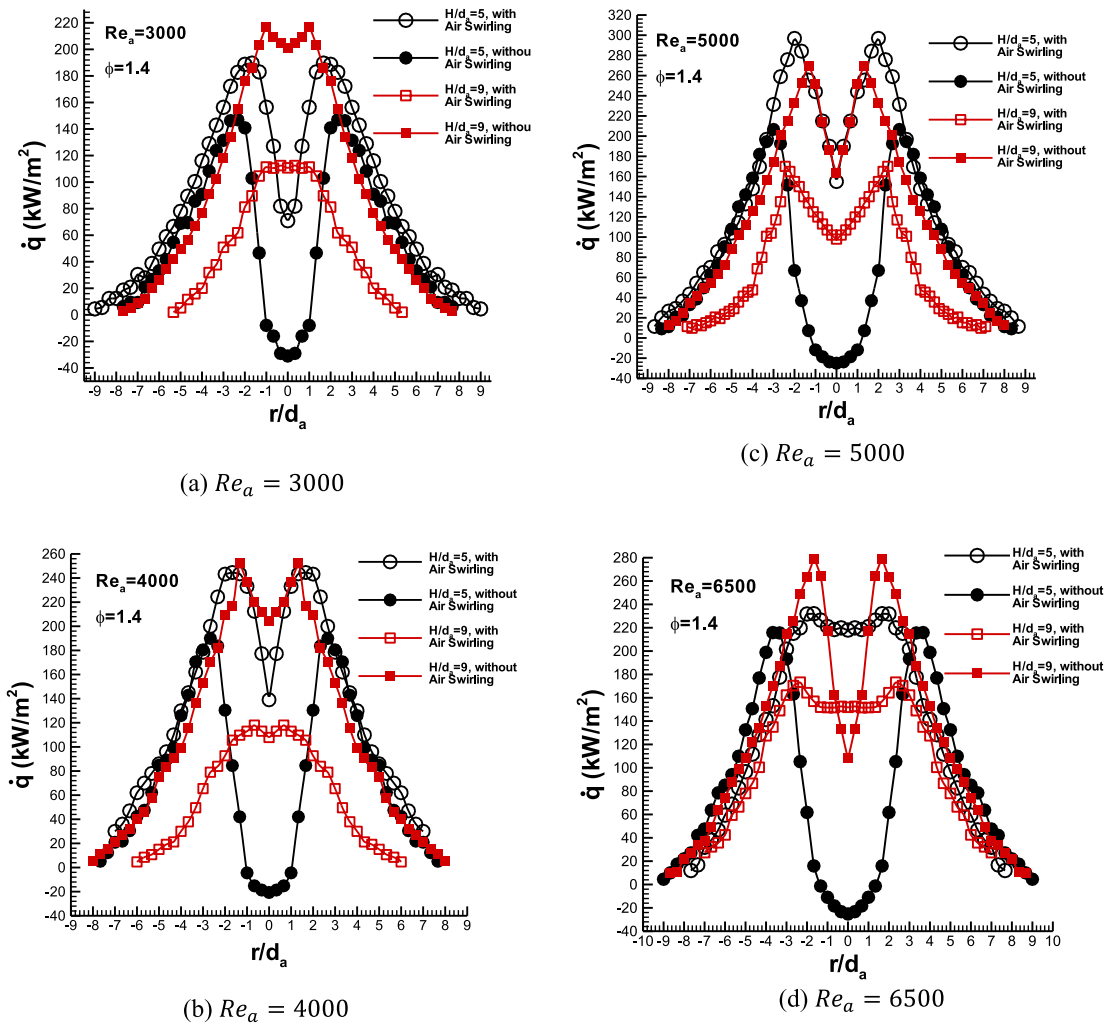

Fig. 11. Comparisons of the Radial Heat Flux Distributions in the Flame Jets with and without Air Swirling

(3) The optimal heat transfer performance with the maximized $\dot{q}$ is obtained when two conditions are met. First, the impingement plate is placed in such a position that the tip of the flame inner reaction zone just touches the plate. Second, the combustion in the inner reaction zone occurs under a nearly stoichiometric condition where the maximum flame temperature is achieved.

(4) Introduction of air swirling can either enhance or reduce the heat transfer rate depending on the specific impingement configuration. Insufficient swirling under low Re_a of 3000 cannot change the yellow diffusion flame structure to a blue premixed one and produce no evident enhancement in heat transfer rate. Over-swirling under high Re_a of 6500 entrains more ambient air and gives rise to a reduction in flame temperature and heat transfer rate. An enhancement in heat transfer rate is only achieved under an appropriate swirling level when a complete combustion around a stoichiometric condition occurs.

(5) By introducing inverse diffusion flame and air swirling, a blue premixed flame torch above the flame neck can be achieved. Therefore, it possesses the advantages of a premixed flame jet with intense heat release rate, high flame temperature, less or no soot emission, and ultra-low NO_x emission. The heat transfer rate is enhanced comparing to non-swirling flame jet as a result of the premixed combustion mode. In the meantime, this flame is a diffusion flame in nature with no danger of flashback. The flame neck in its unique flame structure is able to self-stabilize the premixed flame torch under large Re_a in the fully turbulent flow region. These characteristics give it extra advantages than a premixed flame jet. Therefore, the present experimental study shows that an impinging IDF jet with appropriate level of air swirling is a desirable option for impingement heating.

CRediT authorship contribution statement

L.L. Dong: Conceptualization, Investigation, Writing - original draft. **C.S. Cheung:** Conceptualization, Funding acquisition, Supervision, Writing - review & editing. **C.W. Leung:** Conceptualization, Supervision, Writing - review & editing.

Declaration of Competing Interest

The authors declare that they have no known competing financial interests or personal relationships that could have appeared to influence the work reported in this paper.

Acknowledgement

The authors wish to thank The Hong Kong Polytechnic University and the Research Grants Council of the Hong Kong SAR (Project No. PolyU 5142/05E) for financial support of the present study.

References

[1] C.E. Baukal, B. Gebhart, Heat transfer from oxygen-enhanced natural gas flames impinging normal to a plane surface, Exp. Therm. 765 Fluid Sci. 16 (1998) 247–259.

[2] C.J. Hoogendoorn, Cz.O. Popiel, Th.H. van der Meer, Turbulent heat transfer on a plane surface in impingement round premixed plate jets, in: Canadian Society for Chemical Engineering (Ed.), Int. Heat Transfer Conference, National Research Council of Canada, 1978, pp. 107–112.

[3] E. Buhr, G. Haupt, H. Kremer, Heat Transfer from Impinging Turbulent Jet Flames to Plane Surfaces. Combustion Institute European Symposium 1973E, 1973.

[4] J.W. Mohr, J. Seyed-Yagoobi, R.H. Page, Combustion measurements from an impinging radial jet reattachment flame, Combust. Flame 106 (1996) 69–80.

[5] L.L. Dong, C.W. Leung, C.S. Cheung, Combustion optimization of a slot flame jet impinging system, J. Inst. Energy 76 (2003) 80–88.

[6] J.W. Mohr, J. Seyed-Yagobi, R.H. Page, Optimization of a practical radial jet reattachment flame, in: National Heat Transfer Conference, 1995, pp. 3–10.

[7] H., Koten, M.Yilmaz, M. Z. Gul, Effects of the Injection Parameters and Compression Ratio on the Emissions of a Heavy-Duty Diesel Engine“, International Journal of Vehicle Design, vol. 59 (2/3) (2012), 147-163.

[8] J.W. Mohr, J. Seyed-Yagoobi, R.H. Page, Heat transfer characteristics of a radial jet reattachment flame, J. Heat Transfer 119 (1997) 258–264.

[9] M.E. Horsley, M.R.I. Purvis, A.S. Tariq, Convective heat transfer from laminar and turbulent premixed flames, Heat Transfer 3 (1982) 409–415.

[10] R. Rigey, B.W. Webb, An experimental investigation of diffusion flame jet impingement heat transfer, in: Proceedings of the ASME/ JSME Thermal Engineering Joint Conference, vol. 3, 1995, pp. 117-126. 753.

[11] T.H. van der Meer, Heat transfer from impinging flame jets, Delft university of technology, Netherland, 1987. Ph.D. thesis.

[12] C.J.Hoogendoorn, Cz.O.Popiel, Th.H.van der Meer, 1978, Turbulent Heat Transfer on a Plane Surface in Impingement Round Premixed plate Jets, Int. Heat Transfer Conference, pp. 107-112.

[13] L. Huang, M.S.., El-Genk, Heat Transfer and Flow Visualization Experiments of Swirling, Multi-Channel, and Conventional Impinging Jets, International Journal of Heat and Mass Transfer 41 (3) (1998), 583-600.

[14] J. Ward, M., Mahmood, Heat Transfer from a Turbulent, Swirling, Impinging Jet, 7th International Heat Transfer Conference, Vol. HTD-3, 1982, 401-407.

[15] L. Huang, M.S., El-Genk, Heat Transfer and Flow Visualization of Swirling Impinging Jets, 31st National Heat Transfer Conference, Vol. HTD-324, 1996, 93-1000.

[16] D. Feikema, R., Chen, J.F., Driscoll, Enhancement of Flame Blow-Out Limits by Use of Swirl, Combustion and Flame, 80 (1990), 183-195.

[17] D. Feikema, R., Chen, J.F., Driscoll, Blow-Out of Non-Premixed Flames: Maximum Coaxial Air Velocities Achievable with and without Swirl, Combustion and Flame, 86 (1991), 347-358.

[18] R.H., Chen, Effect of Swirl on the Recirculation within Swirl-Stabilized Flames, Combustion Science and Technology (110-111), 443, 1995.

[19] T. Terasaki, S., Hayashi, Twenty-Sixth Symposium (International) on Combustion, The Combustion Institute, Pittsburgh, 1996, p. 2733.

[20] C.K. Chan, K.S. Lau, W.K. Chin, Freely Propagating Open Premixed Turbulent Flames Stabilized by Swirl, in: 24th International Symposium on Combustion Pittsburgh, 1992, pp. 511–518.

[21] D.H. Lee, S.Y. Won, Y.T. Kim, Y.S. Chung, Turbulent Heat Transfer from a Flat Surface to a Swirling Round Impinging Jet, Int. J. Heat Mass Transf. 45 (2002) 223–226.

[22] X.Q. Huang, C.W. Leung, C.K. Chan, S.D. Probert, Thermal Characteristics of a Premixed Impinging Circular Laiminar-Flame Jet with Induced Swirl, Appl. Energy 83 (4) (2006) 401–411.

[23] S.J. Kline, F.A. McClintock, Describing Uncertainties in Single Sample Experiments, Mech. Eng. 75 (1953) 3–8.

[24] G. Sapra, S. Chander, Effect of Operating and Geometrical Parameters of Tangential Entry Type Dual Swirling Flame Burner on Impingement Heat Transfer, Appl. Therm. Eng. 81 (2020), 115936.

[25] P. Singh, S. Chander, Heat Transfer and Fluid Flow Characteristics of a Pair of Interacting Dual Swirling Flame Jets Impinging on a Flat Surface, Int. J. Heat Mass Transf. 124 (2018) 90–108.

[26] B. Markal, Experimental Investigation of Heat Transfer Characteristics and Wall Pressure Distribution of Swirling Coaxial Confined Impinging Air Jets, Int. J. Heat Mass Transf. 124 (2018) 517–532.

[27] S. Mahesh, D.P. Mishra, Flame stability and emission characteristics of turbulent LPG IDF in a backstep burner, Fuel 87 (2008) 2614.

[28] K.H. Lyle, Tseng LK, Gore JP, Laurendeau NM. A study of pollutant emission characteristics of partially premixed turbulent jet flames. Combustion and Flame 116(1999) 627 - 639.

[29] D. Shen, J.M. Most, P. Joulain, J.S. Bachman, The Effect of Initial Conditions for Swirl Turbulent Diffusion Flame with a Straight-Exit Burner, Combust. Sci. Technol. 100 (1994) 203–224.

[30] R.H. Chen, J.F. Driscoll, The Role of the Recirculation Vortex in Improving Fuel-Air Mixing within Swirling Flames, in: Twenty-Second Symposium (International) on Combustion, The Combustion Institute, Pittsburgh, 1986, p. 1435.

[31] W.P. Partridge, N.M. Laurendeau, Nitric Oxide Formation by Inverse Diffusion Flames in Staged-Air burners, Fuel 74 (10) (1995) 1424–1430.

[32] D.M. Stansel, N.M. Laurendeau, D.W. Senser, CO and NOx emissions from a controlled-air burner: experimental measurements and exhaust correlations, Combust. Sci. Technol. 104 (4–6) (1995) 207–234.

[33] D. Bradley, K.J. Matthews, Measurement of high gas temperatures with fine wire thermocouple, J. Mech. Eng. Sci. 10 (1968) 299–305.

[34] E.M. Sparrow, R.D. Cess, Radiation heat transfer, augmented edition, McGraw-Hill, 1978.